Computation and Analysis of Dielectric Losses in MV Power Electronic Converter Insulation

T. Guillod,
R. Färber,
F. Krismer,
C. Franck,
J. W. Kolar

ETH

Eidgenössische Technische Hochschule Zürich
Swiss Federal Institute of Technology Zurich

Computation and Analysis of Dielectric Losses in MV Power Electronic Converter Insulation

Thomas Guillod*, Raphael Färber†, Florian Krismer*, Christian M. Franck†, and Johann W. Kolar*

*Power Electronic Systems Laboratory (PES)
ETH Zurich
8092 Zurich, Switzerland

†High Voltage Laboratory (HVL)
ETH Zurich
8092 Zurich, Switzerland

Abstract—**The newly available Medium Voltage (MV) Silicon-Carbide (SiC) devices enable a great extension of the design space of MV inverters. This includes the utilization of unprecedented blocking voltages, higher switching frequencies, higher commutation speeds, and high temperature operation. However, all these factors considerably increase the insulation stress. This paper details the computation of dielectric losses, which are directly related to the insulation stress and can be used for the insulation design and diagnostic. After a review of the method used to compute dielectric losses, scalable analytical expressions are derived for the losses produced by PWM waveforms of DC-DC, DC-AC, and multilevel DC-AC inverters. Finally, a Medium-Frequency (MF) transformer is analyzed and the impacts of the insulation material and the operating temperature on the dielectric losses are discussed. It is found that the insulation losses can represent a significant share (17 %) of the total transformer losses.**

Index Terms—**Power Electronics, Dielectrics and Electrical Insulation, Dielectric Losses, Medium-Frequency Transformers, Medium-Voltage Transformers.**

I. INTRODUCTION

The need to integrate renewable energy sources into the MV grid, to supply large loads from the MV grid, or to control the power flow, has led to a rapid growth of the research and industry interest for MV connected power electronic inverters, using MF energy conversion [1]–[3]. The design of such converters is often examined at system level [3], [4] and component level [5]–[8] while the insulation coordination is often neglected [9], [10].

According to [11], insulation failures, for example in connected magnetic components, are already challenging in Low-Frequency (LF) systems. In [12]–[14], it is shown that the fast voltage transients generated by power converters further increase the stresses applied to a dry-type insulation system, leading to increased failure rates. In this context, the usage of new SiC switches, which achieve higher voltage capabilities, higher switching frequencies, and higher switching speeds, is particularly critical [1], [7]. Moreover, due to the high power density, elevated operating temperatures usually apply to power converters. For these reasons, the insulation used in such inverters requires a careful examination in order to obtain a reliable system but also for achieving good thermal and EMI performances.

Literature related to the evaluation of insulation stresses proposes the examination of partial discharges, breakdown voltages, field distributions, dielectric losses, etc. [9], [13]–[15]. Among these methods, the inspection of dielectric losses is of particular interest, since dielectric loss densities are found to be related to the lifetime and the reliability of insulation systems [14]–[17] and because the calculation of dielectric losses is easier than the computation of partial discharge activities or breakdown voltages. Consequently, even if the dielectric losses are usually small compared to the total losses of a converter [9], their computation is still very useful for classifying insulation stresses and materials. Moreover, the online or offline monitoring of the insulation losses allows the detection of insulation degradation and represents a valuable diagnostic tool [16], [18], [19].

This paper examines in detail the computation of insulation losses in converters. **Fig. 1** presents a typical workflow for the computation of the losses where the dependencies between the different parameters are shown. The computation of dielectric losses considers the applied waveforms, the geometry, the temperature distribution, the electric field, and the material properties [15]–[17]. The temperature distribution links the computation of the dielectric losses to the other losses (induced currents, hysteresis, etc.) present in the considered component.

This paper is organized as follows. After the definition of the dielectric losses computation in **Section II**, simple and scalable expressions are derived for the evaluation of the losses for typical converter waveforms in **Section III**: PWM with constant duty cycle, sinusoidal modulation, and multilevel sinusoidal modulation. Finally, in **Section IV**, the presented analysis method is applied to a MV/MF transformer in order to evaluate the insulation stress.

II. DIELECTRIC LOSSES COMPUTATION

The dielectric response of a solid insulation material depends on various microphysical processes such as polarization (e.g. electronic, atomic, dipolar), conduction, charge trapping, etc. [15], [16]. In this paper, the polarization effects are considered to be linear with respect to the electric field, which holds approximately true for most of the materials used for MV insulations [15], [17], [20]. With these assumptions, the dielectric response of an isotropic material is fully described in the frequency domain by the complex permittivity [15], [17], [19]:

$$\varepsilon(f, T) = \varepsilon_0 \left(\varepsilon'(f, T) - j\varepsilon''(f, T) \right), \tag{1}$$

which is dependent on the frequency f and the operating temperature T. This model is not applicable for modeling the response of a material to a DC electric field. However, the DC conduction losses can be neglected since the AC losses are much larger at MF. Furthermore, this model is not able to predict the nonlinearities and the additional losses appearing above the partial discharge inception voltage [12].
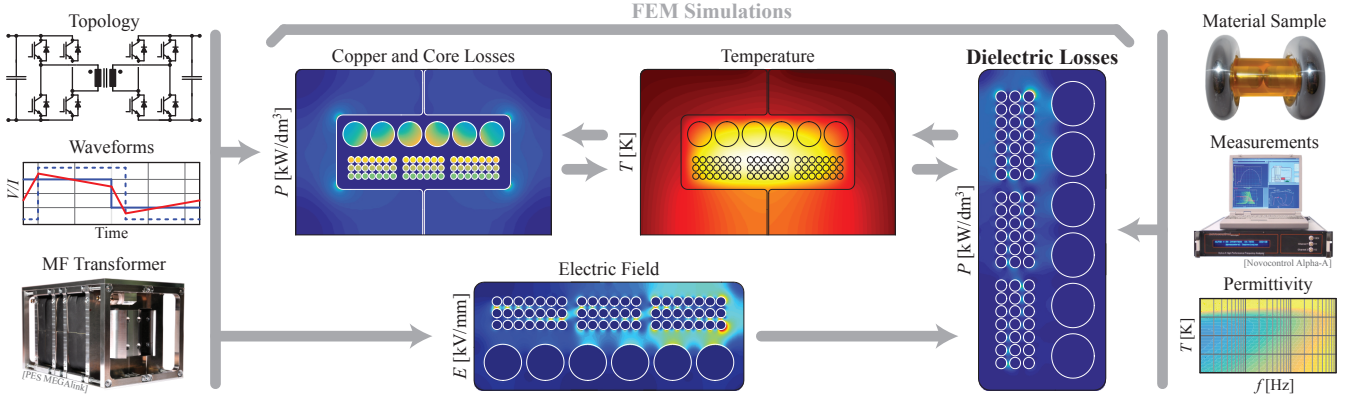
Fig. 1. Workflow for the computation of dielectric losses inside insulation systems. The procedure is here shown for a 4kV MV/MF transformer [1] but can be adapted to busbars, semiconductor packages, filters, etc.

For practical applications, the real part of the permittivity (ε') is often given together with the loss tangent ($\tan\delta$). An equivalent circuit consisting of the series connection of a capacitor (C_{ESR}) and a resistor (R_{ESR}) is also a common model. The corresponding parameters are defined as:

$$\tan\delta = \frac{\varepsilon''}{\varepsilon'}, \tag{2}$$

$$C_{\text{ESR}} = \frac{\varepsilon''^2 + \varepsilon'^2}{\varepsilon'} C_0 \overset{\varepsilon' \gg \varepsilon''}{\approx} \varepsilon' C_0, \tag{3}$$

$$R_{\text{ESR}} = \frac{\varepsilon''}{\varepsilon''^2 + \varepsilon'^2} \frac{1}{2\pi f C_0} \overset{\varepsilon' \gg \varepsilon''}{\approx} \frac{\varepsilon''/\varepsilon'}{2\pi f C_{\text{ESR}}}. \tag{4}$$

The loss tangent is a figure of merit for capacitors (losses compared to the stored energy). Since energy storage is not a desirable property of insulation materials, the loss tangent is not a figure of merit for insulation materials. Models based on the series equivalent circuit are frequency-dependent even for a constant complex permittivity. This means that these models cannot easily be used in the time domain and lead to complex expressions for the dielectric losses. For these reasons, the complex permittivity representation in the frequency domain is used in this paper.

With the help of the complex permittivity, it is possible to express the time-averaged losses of an insulation system excited with a periodic electric field as:

$$P = \iiint_{\text{V}} \left(\sum_{n=1}^{\infty} \varepsilon_0 \varepsilon''(fn, T)(2\pi fn) E_{n,\text{RMS}}^2 \right) dV, \tag{5}$$

where V is the insulation volume, f the fundamental frequency, and $E_{n,\text{RMS}}$ the RMS Fourier series coefficients of the electric field norm. In case of a homogeneous and isothermal dielectric placed between two electrodes, the expression for the losses can be simplified to:

$$P = \sum_{n=1}^{\infty} P_n = C_0 \sum_{n=1}^{\infty} \varepsilon''(fn, T)(2\pi fn) V_{n,\text{RMS}}^2, \tag{6}$$

where C_0 is the vacuum capacitance (computed with ε_0) associated with the geometry and $V_{n,\text{RMS}}$ are the RMS Fourier series coefficients of the applied voltage. This expression can be extended to systems with more than two electrodes by using the capacitance matrix.
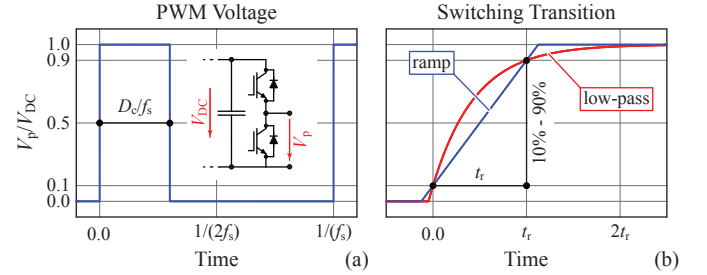
Fig. 2. (a) PWM signal with a constant duty cycle. (b) Two different approximations of the switching transition (rise time t_r): the ramp function and the step response of a first order low-pass filter.

III. DIELECTRIC LOSSES WITH PWM VOLTAGES

Expression (6) facilitates the calculation of the dielectric losses by means of numerical computations. It is, however, very difficult to identify the influence of the different parameters, since the frequency-dependent material parameter $\varepsilon''(f)$ and the amplitude of the voltage harmonic components appear in the product term of the infinite sum.

In order to find a closed-form solution, a constant value of $\varepsilon''(f)$ is considered in Subsections III-A and III-B, which, according to [20], [21] is an admissible assumption for certain insulation materials (in the considered MF range), especially low-loss materials. With this hypothesis, $\varepsilon''(f)$ can be taken out of the sum (6), allowing the decoupling of the impact of the material from the excitation. Afterwards, in Subsection III-C, the impact of the frequency dependence of the permittivity is analyzed.

A. PWM with Constant Duty Cycle

In steady state operation, typical DC-DC converters generate PWM voltages with a constant duty cycle, according to **Fig. 2(a)** [1], [9]. **Fig. 2(b)** proposes two approximations for the switching transition: the commonly used ramp function and the step response of a first order low-pass filter. Since the proposed calculation of the dielectric losses is conducted in the frequency domain, the ramp function is found to be less suitable since it generates a spectrum with side lobes. For this reason, the step response of the following low-pass filter is used:

$$G_{\text{lp}}(f) = \frac{1}{1 + j\frac{f}{f_c}}, \qquad f_c = \frac{\ln\left(\frac{0.9}{0.1}\right)}{2\pi t_r}, \tag{7}$$
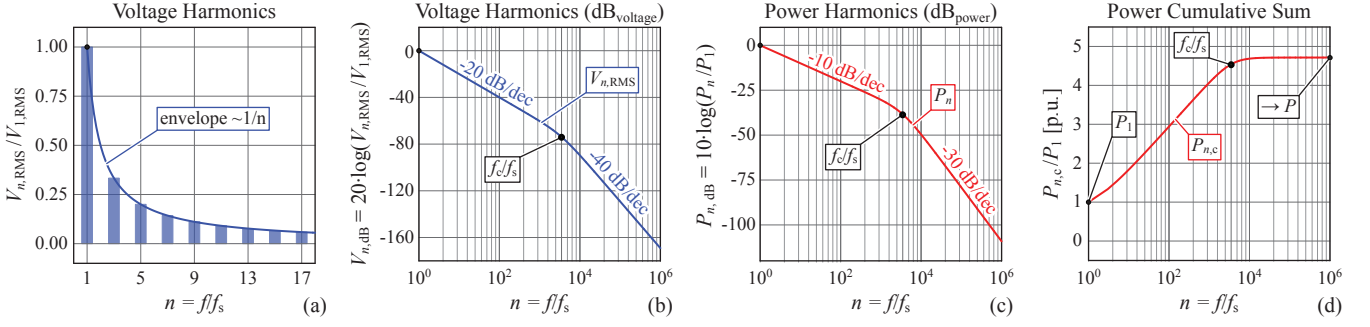
Fig. 3. (a) Voltage harmonics for PWM signal with a constant duty cycle, (b) envelope of the voltage harmonics (in $\mathrm{dB_{voltage}}$), (c) envelope of the power losses harmonics (in $\mathrm{dB_{power}}$), and (d) cumulative sum of the power harmonics. The following parameters are used: $f_s = 1\,\mathrm{kHz}$, $t_r = 100\,\mathrm{ns}$, and $D_c = 0.5$. With the chosen duty cycle, only the odd harmonics are non-zero.

where t_r is the $10\% - 90\%$ rise time, cf. Fig. 2(b). The corresponding harmonic components (Fourier series) of the PWM voltage can be computed as:

$$V_{n,\mathrm{RMS}} = \left(\frac{\sqrt{2}}{\pi} \frac{|\sin(\pi D_c n)|}{n} V_{\mathrm{DC}} \right) |G_{\mathrm{lp}}(f_s n)|, \quad (8)$$

where D_c is the duty cycle, V_{DC} the amplitude, and f_s the switching frequency. From the voltage harmonics, the spectral components of the losses (cf. (6)) can be expressed:

$$P_n = \left(\varepsilon'' C_0 \right) \left(2\pi f_s n \right) V_{n,\mathrm{RMS}}^2. \quad (9)$$

The dielectric losses can be computed as the sum of the spectral components:

$$P = \lim_{n \to \infty} P_{n,c}, \qquad P_{n,c} = \sum_{n'=1}^{n} P_{n'}. \quad (10)$$

where $P_{n,c}$ is the partial losses of the first n harmonics and P the total losses.

Fig. 3 depicts the voltage harmonics (cf. (8)), the losses spectral components (cf. (9)), and the cumulative sum of the losses (cf. (10)). The voltage and power harmonics are proportional to $\sim 1/n$ for frequencies below the corner frequency. Therefore, the sum (10) only converges after the corner frequency of the low-pass filter. This implies that an infinitesimally short switching transition would lead to infinite losses. Therefore a model of the switching transition is required (cf. (7)). Moreover, the sum P is much greater than the fundamental harmonic P_1, showing that a fundamental frequency analysis is inappropriate.

The calculation of (10) is computationally intensive since it requires the summation of many harmonics. Therefore, a closed-form approximation is proposed (with the hypothesis $\varepsilon''(f) = \mathrm{const.}$):

$$P = \left(\varepsilon'' C_0 V_{\mathrm{DC}}^2 \right) P', \quad (11)$$

$$P' \approx \frac{2 f_s}{\pi} \ln \left(\frac{2 e^\gamma f_c}{f_s} \sin(\pi D_c) \right), \quad (12)$$

where $\gamma \approx 0.57$ is the Euler-Mascheroni constant and P' the normalized losses. The derivation of (11) requires elaborate calculations, which are given in **Appendix A**. The accuracy of the approximation is evaluated in **Appendix C** and shows that the approximation is valid (0.1 % error). The error is also small (2.5 % error) if a ramp function is used in place of the
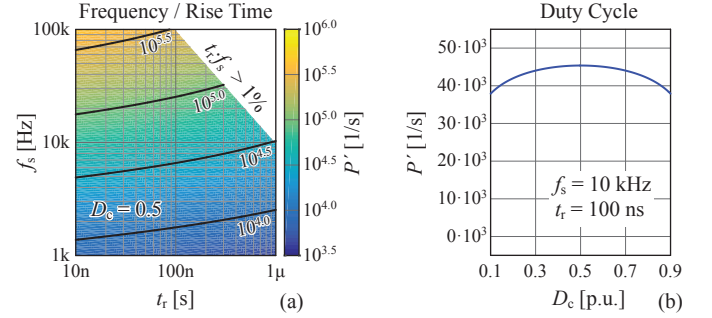
Fig. 4. (a) Impact of the switching frequency, the rise time, and (b) the duty cycle on the dielectric losses. The excitation is a PWM signal with a constant duty cycle. All the power values are normalized with respect to $\varepsilon'' C_0 V_{\mathrm{DC}}^2$ while the used parameters are given in the figures.

TABLE I
PWM WITH CONSTANT DUTY CYCLE.

Param.	Impact on P
f_s	$P \sim f_s \ln(\mathrm{const.}/f_s)$
t_r	$P \sim \ln(\mathrm{const.}/t_r)$
D_c	$P \sim \mathrm{const.}$
V_{DC}	$P \sim V_{\mathrm{DC}}^2$
ε''	$P \sim \varepsilon''$

low-pass filter step response. This indicates that an exact model of the switching transition is not necessarily required and that the model presented in (7) is valid.

Fig. 4(a) depicts the results of (11) for different rise times and switching frequencies. It can be seen that the impact of the frequency is very strong while the losses increase only logarithmically with respect to the reciprocal of the rise time. **Fig. 4(b)** shows that the duty cycle has only a minor impact on the dielectric losses. The impact of the different parameters on the losses are summarized in **Tab. I**.

B. PWM with Sinusoidal Modulation

Since many MV converters are connected to the grid, it is also important to evaluate the insulation losses with LF and MF excitations (mixed-frequency voltage stress) [3], [9], [18]. Since the corner frequency (cf. (7)) is much greater than the grid frequency, the numerical computation of the dielectric losses requires a very high number of harmonics (more than 10^5 for a grid frequency of 50 Hz with rise times below 100 ns). This, especially, leads to a computationally
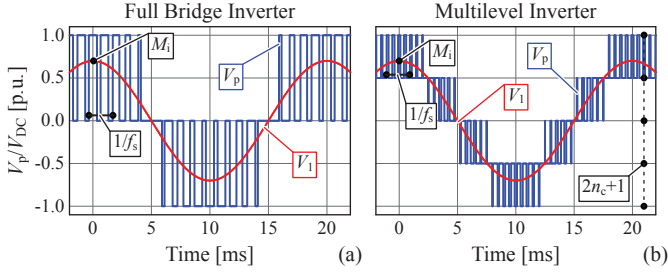
Fig. 5. (a) PWM waveform produced by a full-bridge inverter. (b) Multilevel PWM waveform produced by n_c cascaded full-bridges (shown for $n_\mathrm{c} = 2$).

TABLE II
PWM WITH SINUSOIDAL MODULATION.

Param.	Impact on P_1	Impact on P_harm
f_s	$P \sim \mathrm{const.}$	$P \sim f_\mathrm{s} \ln\left(\mathrm{const.}/f_\mathrm{s}\right)$
f_g	$P \sim f_\mathrm{g}$	$P \sim \mathrm{const.}$
t_r	$P \sim \mathrm{const.}$	$P \sim \ln\left(\mathrm{const.}/t_\mathrm{r}\right)$
M_i	$P \sim M_\mathrm{i}^2$	$P \sim \mathrm{const.}$
n_c ($f_\mathrm{s} = \mathrm{const.}$)	$P \sim \mathrm{const.}$	$P \sim (1/n_\mathrm{c}) \ln\left(\mathrm{const.}/n_\mathrm{c}\right)$
n_c ($f_\mathrm{e} = \mathrm{const.}$)	$P \sim \mathrm{const.}$	$P \sim 1/n_\mathrm{c}^2$
V_DC	$P \sim V_\mathrm{DC}^2$	$P \sim V_\mathrm{DC}^2$
ε''	$P \sim \varepsilon''$	$P \sim \varepsilon''$

intensive situation when a volume integration of the losses is required (cf. (5)).

It has been found that the scope of application of (11) can be extended to inverters with sinusoidal modulation by means of local averaging. For the voltage waveforms produced by a single-phase full-bridge inverter, cf. **Fig. 5(a)**, the following approximation is derived (with the hypothesis $\varepsilon''(f) = \mathrm{const.}$):

$$P = P_1 + P_\mathrm{harm} = \left(\varepsilon'' C_0 V_\mathrm{DC}^2\right)\left(P_1' + P_\mathrm{harm}'\right), \qquad (13)$$

$$P_1' = \left(2\pi f_\mathrm{g}\right)\left(\frac{M_\mathrm{i}}{\sqrt{2}}\right)^2 = \pi f_\mathrm{g} M_\mathrm{i}^2, \qquad (14)$$

$$P_\mathrm{harm}' \approx \lim_{\epsilon \to 0} \int_{0+\epsilon}^{1-\epsilon} \left(\frac{2 f_\mathrm{e}}{\pi} \ln\left(\frac{2 e^\gamma f_\mathrm{c}}{f_\mathrm{e}} \sin\left(\pi D_\mathrm{c}\left(\xi\right)\right)\right)\right) \mathrm{d}\xi, \qquad (15)$$

$$D_\mathrm{c}\left(\xi\right) = M_\mathrm{i} \sin\left(\frac{\pi}{2}\xi\right), \qquad f_\mathrm{e} = 2 f_\mathrm{s}, \qquad (16)$$

where f_g is the grid frequency, f_s the switching frequency of the semiconductors, f_e the effective switching frequency of the output AC signal, and M_i the modulation index.

Due to the limited voltage capabilities of MV semiconductors, multilevel converter structures are often used [9], [22]. **Fig. 5(b)** shows a typical multilevel waveform produced by n_c cascaded full-bridges (with phase-shifted PWM carriers) producing $2n_\mathrm{c} + 1$ levels. The local averaging of (11) is also applicable to multilevel waveforms where the effective switching frequency is $f_\mathrm{e} = 2n_\mathrm{c} f_\mathrm{s}$. The local duty cycle, $D_\mathrm{c}\left(\xi\right)$, is a piecewise defined function. A case differentiation is required due to the fact that, for low modulation indexes, only a reduced set of the available voltage levels is used. For this reason, a simple expression for $D_\mathrm{c}\left(\xi\right)$ does not exist.

The accuracy of these approximations is evaluated in **Appendix C** and shows that the local averaging of the duty cycle is valid for both single and cascaded inverters (3.4 % error).

Figs. 6(a) and (b) depict the losses for different modulation indexes. The losses at the grid frequency are proportional to the square of the modulation index and independent of the number of levels. The losses of the higher harmonics are not strongly dependent on the modulation index. It has to be noted that P_harm' is much greater than P_1'. With n_c cascaded full-bridges, P_harm' oscillates n_c times when evaluated over the modulation index. As explained above, this is due to the piecewise definition of $D_\mathrm{c}\left(\xi\right)$.

Fig. 6(c) shows that the dependence of the losses on the switching frequency is similar to the case shown in Fig. 4(a). The obtained results reveal that the dielectric losses of the higher harmonics can be greatly reduced with

multilevel inverters. This is due to the reduction of the voltage steps produced by multilevel waveforms, which is, however, mitigated by the increase of the effective switching frequency. If the number of levels is increased with a constant effective switching frequency, an even greater reduction of the losses results. This highlights one advantage of multilevel inverters for MV applications [22].

The impact of the different parameters on the losses (P_1 and P_harm) are summarized in **Tab. II** for cascaded full-bridges with phase-shifted PWM carriers.

C. PWM with Frequency-Dependent Materials

Until now, a constant $\varepsilon(f)$ has been assumed. This assumption, however, may be inaccurate for some materials, especially for epoxy resins which are frequently used for MV insulations. In this paper, a typical MV insulation epoxy resin has been chosen (Damisol 3418, with glass transition temperature: $T_\mathrm{g} = 136\,°\mathrm{C}$ [23]). **Fig. 7** shows the measured ε' and ε'' for the chosen resin where the material parameters are strongly frequency and temperature dependent. The losses are particularly high for temperatures near the glass transition temperature [24], [25]. The measurements are done with a disc-shaped specimen using a Novocontrol Alpha-A Analyzer (cf. Fig. 1) [26].

In Subsections III-A and III-B, it has been shown that the influence of the duty cycle and the modulation index on the losses is moderate. For this reason, a signal with a constant duty cycle ($D_\mathrm{c} = 0.5$) is chosen. With this assumption, a closed-form approximation can be found:

$$P \approx \left(C_0 V_\mathrm{DC}^2\right)\left(P_\mathrm{add}' + P_\mathrm{int}'\right), \qquad (17)$$

$$P_\mathrm{add}' = \frac{2 f_\mathrm{s}}{\pi} \ln\left(2 e^\gamma\right) \varepsilon''\left(f_\mathrm{s}\right), \qquad (18)$$

$$P_\mathrm{int}' = \frac{2 f_\mathrm{s}}{\pi} \underbrace{\int_{\ln(f_\mathrm{s})}^{\ln(f_\mathrm{c})} \varepsilon''\left(f\right) \mathrm{d}\left(\ln\left(f\right)\right)}_{\varepsilon_\mathrm{int}''}. \qquad (19)$$

The derivation of (17) is given in **Appendix B**. The proposed formula requires the measurement of $\varepsilon''(f)$, which is not always available and difficult to measure (due to $\varepsilon' \gg \varepsilon''$) [16], [24]. However, the real and imaginary parts of the permittivity are linked by the Kramers-Kronig relations [25], [27]. These relations can be locally expressed as:

$$\varepsilon''\left(f\right) \approx -\frac{\pi}{2} \frac{\partial \varepsilon'\left(f\right)}{\partial \ln\left(f\right)}. \qquad (20)$$

It has to be noted that this relation is inaccurate for
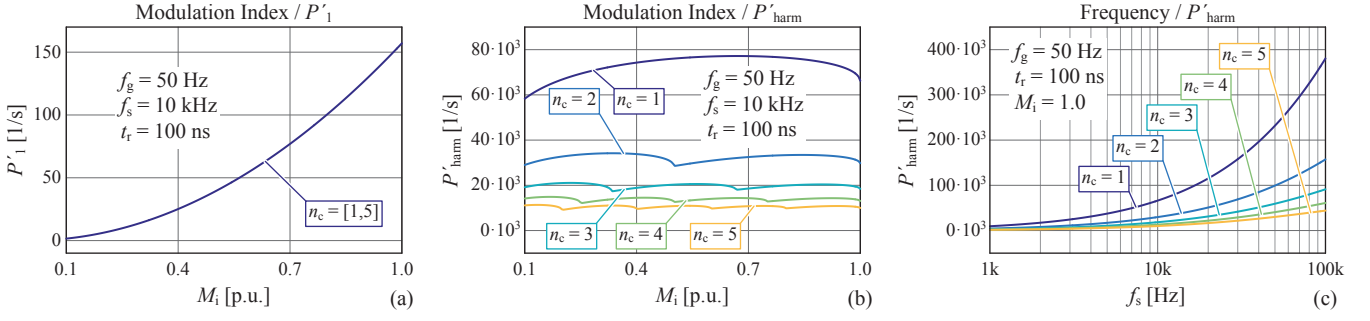
Fig. 6. (a) Impact of the modulation index on the dielectric losses of the fundamental harmonic and (b) of the higher harmonics. (c) Impact of the switching frequency on the dielectric losses of the higher harmonics. The excitation is a PWM signal with sinusoidal modulation produced by n_c cascaded full-bridges. All the power values are normalized with respect to $\varepsilon'' C_0 V_{DC}^2$ while the used parameters are given in the figures.
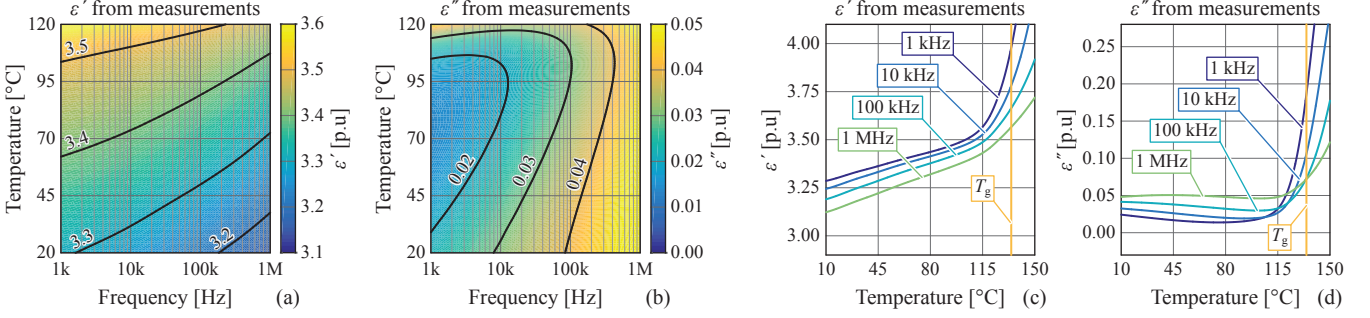
Fig. 7. (a) $\varepsilon'(f,T)$ and (b) $\varepsilon''(f,T)$ measured for the epoxy resin Damisol 3418 for typical operating temperatures. (c) Measured $\varepsilon'(f,T)$ and (d) $\varepsilon''(f,T)$ for an extended temperature range including the glass transition temperature $T_g = 136\,°C$.
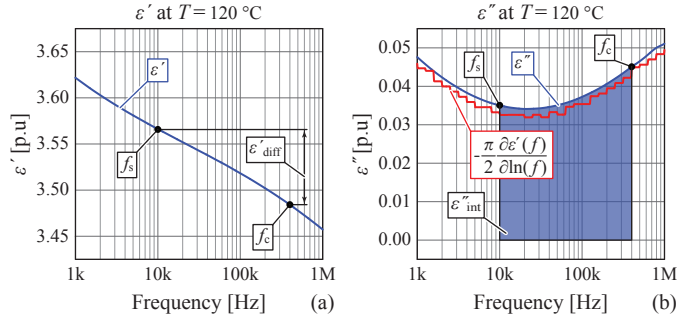
Fig. 8. (a) Measured $\varepsilon'(f)$ and (b) $\varepsilon''(f)$ at 120°C (blue curves). An approximation of $\varepsilon''(f)$, computed with the Kramers-Kronig relations, is also shown (red curve). The area ε''_{int} (cf. (19)) and the difference ε'_{diff} (cf. (23)) are figures of merit for the losses produced by a material.

quantifying the loss peak associated with the glass transition temperature of the material (cf. Fig. 7). However, for the chosen resin, the glass transition temperature is above the typical operating temperature of power electronic components such that the Kramers-Kronig relations can be used. With (20), the approximation (17) can be rewritten as:

$$P \approx \left(C_0 V_{DC}^2\right)\left(P'_{add} + P'_{int}\right), \tag{21}$$

$$P'_{add} = -f_s \ln\left(2e^\gamma\right) \left.\frac{\partial \varepsilon'(f)}{\partial \ln(f)}\right|_{f_s}, \tag{22}$$

$$P'_{int} = f_s \underbrace{\left(\varepsilon'(f_c) - \varepsilon'(f_s)\right)}_{\varepsilon'_{diff}}. \tag{23}$$

The area ε''_{int} (cf. (19)) and the difference ε'_{diff} (cf. (23)) are figures of merit for the losses produced by a material and are shown in **Fig. 8**. The measured imaginary part of

the permittivity is compared to the value obtained with (20), showing that the Kramers-Kronig relations hold true.

The accuracy of the approximations (17) and (21) is evaluated in **Appendix C**. Both expressions are found to be valid for the chosen resin (7% error). If the frequency dependence of the material parameters is neglected (cf. (11)), the error is greater than 50%, indicating that the frequency dependence of the permittivity must be considered for accurate computations.

IV. CASE STUDY: MV/MF TRANSFORMER

With the help of the approximations proposed above, the dielectric losses of different components can be examined. Since it has been identified that the stresses are particularly high for MV/MF transformers [8], [9], this component has been chosen.

A. Transformer Design

The proposed method is applied to the 4 kV/400 V, 50 kHz, 25 kW MV/MF transformer of the single-stage MV SiC Solid-State Transformer (SST) presented in [1]. The transformer is used inside a Dual Active Bridge (DAB) DC-DC converter. This transformer has been chosen since it is subject to all identified critical aspects, i.e. in particular high frequency and high voltage operation. The characteristic properties of the transformer are summarized in **Tab. III**.

The voltage and current excitations of the transformer are computed using phase shift modulation (30° at nominal power) [28]. The switching transitions feature Zero Voltage Switching (ZVS) and are modeled as presented in Subsection III-A. The current dependency of the switching speed is considered according to [7].
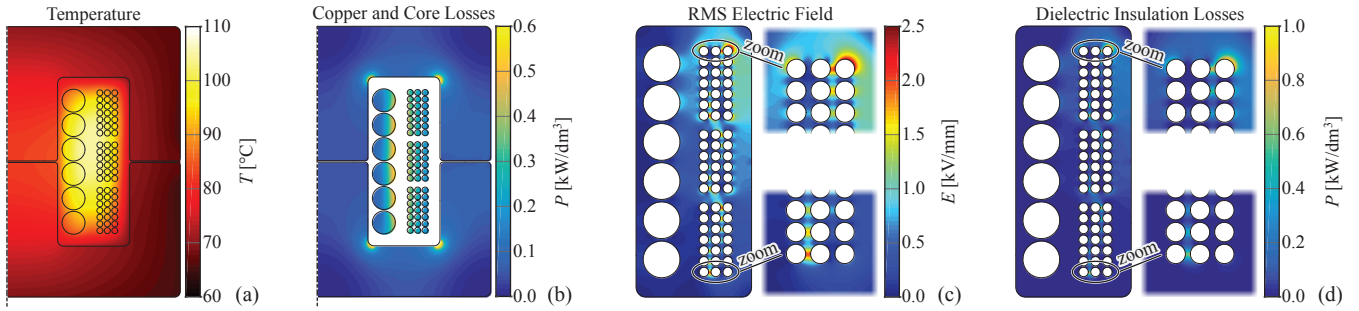
Fig. 9. (a) Temperature distribution, (b) core and windings loss densities, (c) RMS value of the electric field, and (d) dielectric loss density in the insulation computed with the measured material parameters. The simulations are conducted at rated conditions (25 kW).
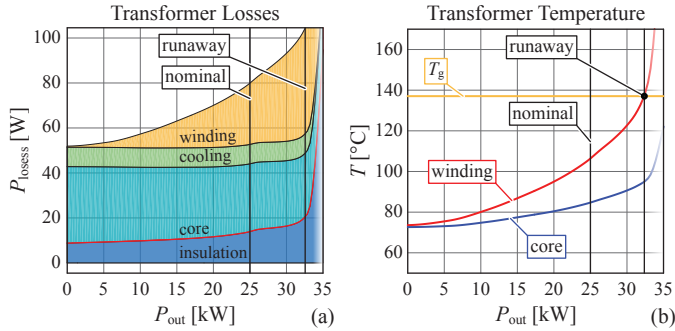
Fig. 10. (a) Transformer loss breakdown for different load conditions. (b) Windings and core hot spot temperatures. The nominal load and the load where a thermal runaway occurs are shown. The glass transition temperature of the insulation material ($T_g = 136\,°C$) is also indicated.

TABLE III
PARAMETERS OF THE MV/MF TRANSFORMER.

Power	25 kW
Voltage	±4 kV / ±400 V
Frequency	50 kHz
Rise time	1000 ns @ 0 kW / 170 ns @ 25 kW / ZVS
Winding	60 : 6 turns / litz wire / shell-type
Wire	$3000 \times 100\,\mu m$ / $380 \times 71\,\mu m$
Core type	ferrite N87 / E-core / $2300\,mm^2$
Core window	$32 \times 65\,mm$
Volume	$120 \times 130 \times 140\,mm$ / $2.2\,dm^3$
Cooling	conduction / forced convection / 50°C ambient
Insulation	epoxy resin / Damisol 3418 / 4 mm thickness

The transformer has been designed following the guidelines proposed in [6]. The magnetic field, the electric field, and temperature are computed with a 2D Finite Element Method (FEM), according to the workflow presented in Fig. 1. The spatial dependence of the losses and the temperature dependence of the material parameters are considered. An iterative process is used in order to link the temperature distribution with the losses. The winding losses (skin and proximity effects) are computed according to [28], the core losses (improved generalized Steinmetz equation) according to [29], and the dielectric losses according to Subsection III-C.

B. Transformer Losses

The corresponding temperature, electric field, and loss distributions are depicted in **Fig. 9** at rated conditions (25 kW). The hot spot temperature (105 °C) is clearly located inside the windings due to the thermal resistance of the insulation. Due

to the inhomogeneous electrode configuration, the electric field is mostly located near the MV winding. The maximal RMS electric field is in a typical range for MV insulation (2.5 kV/mm) [9]. Since the insulation losses are proportional to the square of the electric field (cf. (5)), the dielectric losses are only significant near the surface of the medium voltages winding. The maximum dielectric loss density is even larger than the core and winding loss densities, which indicates that insulation losses are critical.

In order to get a better insight on the transformer losses, the loss densities depicted in Fig. 9 are integrated over the transformer volume. **Fig. 10(a)** shows the obtained losses for different load conditions and **Fig. 10(b)** depicts the corresponding hot spot temperatures. As expected, the voltage related losses (core, cooling, and insulation) are approximately load independent. Only the winding losses, which are related to the current, are strongly load dependent. At rated conditions (25 kW), the total losses are 82 W (efficiency of 99.65 %).

C. Dielectric Losses

At rated conditions (25 kW), the total dielectric losses are 14 W which represent 17 % of the total losses. For the computation of the dielectric losses the following remarks should be considered:

- If the dielectric losses are neglected, an error of 17 % results for the total losses and 10 °C for the hot spot temperature. This means that the dielectric losses cannot be neglected for an accurate transformer simulation.
- If the dielectric losses are computed with a fundamental frequency analysis, an error of 9 W (65 %) results. Therefore, the actual rectangular voltage waveforms must be considered with a model of the switching transition.
- If the approximation of a frequency-independent permittivity is done, an error of 4.5 W (30 %) results for the insulation losses. If the dielectric losses are computed without a thermal model, the error reaches 3.5 W (25 %). This illustrates the importance of the temperature and frequency dependence of the permittivity.

A closer look at the insulation losses (cf. Fig. 10(a)) shows a moderate increase of these losses for loads between 0 kW and 33 kW. This is due to the temperature variation (cf. Fig. 10(b)) and to the increased switching speed of the semiconductors (ZVS with increased current, cf. Tab. III).

For loads exceeding 33 kW (33 % overload), a thermal runaway occurs. The mechanism of the thermal runaway

can be explained as follows. The hot spot temperature of the transformer increases when evaluated over the load. This temperature increase is mainly produced by the winding losses which are strongly load dependent. When the hot spot temperature reaches the glass transition temperature of the insulation material ($T_g = 136$°C for the chosen resin), a massive increase of the dielectric losses occurs (cf. Fig. 7). Due to the high density of insulation losses (cf. Fig. 9), this leads to a thermal runaway.

According to these results, the considered epoxy resin, which is a typical resin employed for low-frequency systems, is less suitable at MF. This is explained by the fact that that the dielectric are non-negligible at MF and very high for operating temperatures close to the glass transition temperature. This will be the case for most epoxy resins with typical glass transition temperatures ranging from 60°C to 140°C [16], [21], [23].

For this reason, materials with significantly lower or higher glass transition temperatures (compared to the operating temperature) would be well-suited for the insulation of MF transformers. For example, the glass transition temperature of silicone elastomers is below 0°C, such that the loss peak near the glass transition temperature is not critical [30]. Furthermore, silicone elastomers feature low dielectric losses at MF and good thermal properties.

V. Conclusion

This paper derives closed-form analytical expressions for calculating the dielectric losses of the materials used in dry-type insulation systems. The proposed approach applies to typical PWM voltages of DC-DC and AC-DC converters. An extension for materials with frequency-dependent losses is also derived. The proposed approximations are verified with permittivity measurements conducted for a typical MV insulation epoxy resin at different frequencies and temperatures.

It is shown that fundamental frequency analysis inaccurately determines the dielectric losses and that finite rise and fall times of the excitation voltage limit the losses. A detailed investigation reveals that the losses in the insulation mainly depend on the voltage amplitude, the switching frequency, and the material parameters. The duty cycle and the modulation index of PWM waveforms have only a minor impact on the insulation losses. Moreover, multilevel inverters exhibit a significant reduction of the losses.

The described computation techniques are applied to a 4 kV/400 V, 50 kHz SST MF transformer (single-stage converter) with a frequency and temperature-dependent model. At nominal operation, the insulation losses (epoxy resin) reach 17% of the total transformer losses, which reveals that an accurate computation of the dielectric losses is required for MV/MF applications. Moreover, the dielectric losses can lead to a thermal runaway of the transformer. It is concluded that typical low-frequency insulation materials are unsuitable for MF excitations. For this reason, future research will investigate alternative insulation concepts and materials, such as silicone elastomers, for MF transformers in more detail.

Appendix

A. PWM with Constant Duty Cycle

This is the derivation of (11). From (10) and (9), the normalized losses P' can be written as (with the hypothesis $\varepsilon''(f) = \text{const.}$):

$$P' = \frac{P}{\varepsilon'' C_0 V_{\text{DC}}^2} = \sum_{n=1}^{\infty} \frac{4 f_s}{\pi} \frac{\sin^2(\pi D_c n)}{n} \frac{1}{1 + \left(\frac{f_s}{f_c} n\right)^2}. \tag{24}$$

The infinite summation can be approximated by a finite summation (until the corner frequency of the first order low-pass filter, cf. (7)). The following summation is derived (using the double angle trigonometric formula):

$$P' \approx \sum_{n=1}^{\lceil f_c/f_s \rceil} \frac{4 f_s}{\pi} \frac{1 - \cos(2\pi D_c n)}{2n}, \tag{25}$$

which can be rewritten as:

$$P' \approx \frac{2 f_s}{\pi} \left(\sum_{n=1}^{\lceil f_c/f_s \rceil} \frac{1}{n} - \sum_{n=1}^{\lceil f_c/f_s \rceil} \frac{(-1)^n \cos(2\pi D_c n - \pi n)}{n} \right). \tag{26}$$

An approximation exists for the partial sum of the first term [31]. The second term converges quickly such that the finite sum can be approximated with the infinite sum, for which a closed-form solution exists [32]. This leads to:

$$P' \approx \frac{2 f_s}{\pi} \left(\ln\left(\frac{f_c}{f_s}\right) + \gamma + \frac{1}{2} \ln(2 + 2\cos(2\pi D_c - \pi)) \right), \tag{27}$$

which is equivalent to the expression (11) (after using the double angle trigonometric formula).

B. PWM with Frequency-Dependent Materials

This is the derivation of (17). From (10) and (9), the normalized losses P' can be written as ($D_c = 0.5$):

$$P' = \frac{P}{C_0 V_{\text{DC}}^2} = \sum_{n=1}^{\infty} \frac{4 f_s}{\pi} \frac{\varepsilon''(f_s n) \cdot \sin^2\left(\frac{\pi}{2} n\right)}{n} \frac{1}{1 + \left(\frac{f_s}{f_c} n\right)^2}. \tag{28}$$

Only the odd harmonics are non-zero. Similar to Appendix A, the summation is truncated at the corner frequency:

$$P' \approx \sum_{n=1\,(\text{odd})}^{\lceil f_c/f_s \rceil} \frac{4 f_s}{\pi} \frac{\varepsilon''(f_s n)}{n}. \tag{29}$$

This summation can be approximated with an integral [33]. The inaccuracy of this approximation near the fundamental frequency is compensated by an additional term P'_{add}:

$$P' \approx P'_{\text{add}} + \underbrace{\frac{1}{2} \frac{4 f_s}{\pi} \int_{\ln(f_s)}^{\ln(f_c)} \varepsilon''(f) \, d(\ln(f))}_{P'_{\text{int}}}, \tag{30}$$

where the factor 1/2 results from the fact that only odd values of n are considered. The term P'_{add} is chosen such that the approximation is equivalent to (11) for the special case of a frequency-independent $\varepsilon''(f)$ (cf. (27) with $D_c = 0.5$). This leads to:

$$P'_{\text{add}} = \frac{2 f_s}{\pi} \left(\gamma + \frac{1}{2} \ln(2 + 2) \right) \varepsilon''(f_s), \tag{31}$$

which, together with (30), is equal to the expression (17).

C. Accuracies of the Proposed Approximations

The accuracy of the following approximations is considered: PWM with constant duty cycle (cf. (11)), PWM with sinusoidal modulation (cf. (13)), frequency-dependent $\varepsilon''(f)$ (cf. (17)), and frequency-dependent ε' (cf. (21)). For these approximations, the switching transitions are modeled with the step response of a first order low-pass filter (cf. (7)).

The aforementioned approximations are compared to the summation (6). For the summation, two approximations of the switching transitions are used (cf. Fig. 2(b)): the ramp function ("ramp") and the step response of a first order low-pass filter ("low-pass").

The considered parameter combinations are shown in **Tab. IV** and are based on typical values used for MV converters. The obtained maximum relative errors are shown in **Tab. V**.

REFERENCES

[1] D. Rothmund, G. Ortiz, T. Guillod, and J. W. Kolar, "10kV SiC-Based Isolated DC-DC Converter for Medium Voltage-Connected Solid-State Transformers," in *Proc. of the IEEE Applied Power Electronics Conf. and Expo. (APEC)*, Mar. 2015, pp. 1096–1103.

[2] C. Zhao, D. Dujic, A. Mester, J. K. Steinke *et al.*, "Power Electronic Traction Transformer - Medium Voltage Prototype," *IEEE Trans. Ind. Electron.*, vol. 61, no. 7, pp. 3257–3268, Jul. 2014.

[3] D. Rothmund, G. Ortiz, and J. W. Kolar, "SiC-based Unidirectional Solid-State Transformer Concepts for Directly Interfacing 400V DC to Medium-Voltage AC Distribution Systems," in *Proc. of the IEEE Telecommunications Energy Conf. (INTELEC)*, Sep. 2014, pp. 1–9.

[4] A. Q. Huang, M. L. Crow, G. T. Heydt, J. P. Zheng, and S. J. Dale, "The Future Renewable Electric Energy Delivery and Management (FREEDM) System: The Energy Internet," *Proc. IEEE*, vol. 99, no. 1, pp. 133–148, Jan. 2011.

[5] L. Heinemann, "An Actively Cooled High Power, High Frequency Transformer with High Insulation Capability," in *Proc. of the IEEE Applied Power Electronics Conf. and Expo. (APEC)*, 2002, pp. 352–357.

[6] G. Ortiz, M. Leibl, J. W. Kolar, and O. Apeldoorn, "Medium Frequency Transformers for Solid-State-Transformer Applications - Design and Experimental Verification," in *Proc. of the IEEE Conf. Power Electronics and Drive Systems (PEDS)*, Apr. 2013, pp. 1285–1290.

[7] D. Rothmund, D. Bortis, and J. W. Kolar, "Accurate Transient Calorimetric Measurement of Soft-Switching Losses of 10kV SiC MOSFETs," in *Proc. of the IEEE Power Electronics for Distributed Generation Systems Symp. (PEDG)*, 2016.

[8] F. Kieferndorf, U. Drofenik, F. Agostini, and F. Canales, "Modular PET, Two-Phase Air-Cooled Converter Cell Design and Performance Evaluation with 1.7kV IGBTs for MV Applications," in *Proc. of the IEEE Applied Power Electronics Conf. and Expo. (APEC)*, Mar. 2016, pp. 472–479.

[9] T. Guillod, J. E. Huber, G. Ortiz, A. De *et al.*, "Characterization of the Voltage and Electric Field Stresses in Multi-Cell Solid-State Transformers," in *Proc. of the IEEE Energy Conversion Congr. and Expo. (ECCE)*, Sep. 2014, pp. 4726–4734.

[10] S. B. Y. Du, G. Wang, and S. Bhattacharya, "Design Considerations of High Voltage and High Frequency Transformer for Solid State Transformer Application," in *Proc. of the Industrial Electronics Society Conf. (IECON)*, Nov. 2010, pp. 421–426.

[11] J. Jagers and S. Tenbohlen, "Evaluation of Transformer Reliability Data Based on National and Utility Statistics," in *Proc. of the Int. Symposium on High Voltage Engineering*, 2009.

[12] D. Fabiani, G. C. Montanari, and A. Contin, "Aging Acceleration of Insulating Materials for Electrical Machine Windings Supplied by PWM in the Presence and in the Absence of Partial Discharges," in *Proc. of the IEEE Conf. on Solid Dielectrics (ICSD)*, 2001, pp. 283–286.

[13] D. Konig, N. Hardt, and V. Scherb, "Comparitive Insulation Tests with DC and AC at 50 Hz and 50 kHz," in *Proc. of the IEEE Conf. on Electrical Insulation and Dielectric Phenomena (CEIDP)*, 1998, pp. 702–705.

[14] P. Wang, A. Cavallini, and G. Montanari, "The Influence of Repetitive Square Wave Voltage Parameters on Enameled wire Endurance," *IEEE Trans. Dielectr. Electr. Insul.*, vol. 21, no. 3, pp. 1276–1284, Jun. 2014.

[15] W. S. Zaengl, "Dielectric Spectroscopy in Time and Frequency Domain for HV Power Equipment I. Theoretical Considerations," *IEEE Elect. Insul. Mag.*, vol. 19, no. 5, pp. 5–19, Sep. 2003.

[16] R. Bartnikas, *Engineering Dielectrics: Measurement Techniques. Electrical Properties of Solid Insultaing Materials. Vol. IIB.* ASTM, 1987.

[17] B. Sonerud, T. Bengtsson, J. Blennow, and S. M. Gubanski, "Dielectric Heating in Insulating Materials Subjected to Voltage Waveforms with High Harmonic Content," *IEEE Trans. Dielectr. Electr. Insul.*, vol. 16, no. 4, pp. 926–933, Aug. 2009.

[18] M. Birle and C. Leu, "Breakdown of Polymer Dielectrics at High Direct and Alternating Voltages Superimposed by High Frequency High Voltages," in *Proc. of the IEEE Conf. on Solid Dielectrics (ICSD)*, 2013, pp. 656–661.

[19] K. Niayesh and E. Gockenbach, "On the Aging Mechanism of Solid Insulating Materials Exposed to Repetitive High Voltage Pulses," *IEEE Trans. Dielectr. Electr. Insul.*, vol. 21, no. 1, pp. 304–310, Feb. 2014.

[20] M. A. Silaghi, *Dielectric Material.* InTech, 2003.

[21] W. B. Westphal and A. Sils, *Dielectric Constant and Loss Data.* Air Force Materials Laboratory, Air Force Systems Command, 1972.

[22] J. E. Huber and J. W. Kolar, "Optimum Number of Cascaded Cells for High-Power Medium-Voltage Multilevel Converters," in *Proc. of the IEEE Energy Conversion Congr. and Expo. (ECCE)*, Sep. 2013, pp. 359–366.

[23] *Damisol 3418 API*, von Roll, Nov. 2013.

[24] F. Kremer and A. Schönhals, *2 Broadband Dielectric Measurement Techniques (10-6 Hz to 1012 Hz).* Springer, 2012.

[25] C. J. F. Böttcher and P. Bordewijk, *Theory of Electric Polarization, Dielectrics in Time-Dependent Fields, Vol. II.* Elsevier, 1978.

[26] Novocontrol Technologies, "Alpha-A, Technical Specification," 2010. [Online]. Available: http://www.novocontrol.de/pdf_s/alph_a_spec.pdf

[27] A. K. Jonscher, "Dielectric Loss under Transient Excitation," *Journal of Physics C: Solid State Physics*, vol. 11, no. 14, p. 601, 1978.

[28] F. Krismer, "Modeling and Optimization of Bidirectional Dual Active Bridge DC–DC Converter Topologies," Ph.D. dissertation, ETH Zurich, 2010.

[29] K. Venkatachalam, C. R. Sullivan, T. Abdallah, and H. Tacca, "Accurate Prediction of Ferrite Core Loss with Nonsinusoidal Waveforms using only Steinmetz Parameters," in *Proc. of the IEEE Workshop on Computers in Power Electronics*, Jun. 2002, pp. 36–41.

[30] C. Johansson and M. Robertsson, "Broadband Dielectric Characterization of a Silicone Elastomer," *Journal of Electronic Materials*, vol. 36, no. 9, pp. 1206–1210, 2007.

[31] G. H. Hardy and E. M. Wright, *An Introduction to the Theory of Numbers.* Oxford University Press, 1979, Ch. 18.

[32] H. B. Dwight, *Tables of Integrals and Other Mathematical Data; Fourth Edition.* Macmillan Company, 1966, Eqn. 418.

[33] F. B. Hildebrand, *Introduction to Numerical Analysis.* McGraw-Hill, New York, 1974, Ch. 5.8.